Ore Geology Reviews 65 (2015) 955–967

Contents lists available at ScienceDirect

Ore Geology Reviews

journal homepage: www.elsevier.com/locate/oregeorev

A laser ablation ICP-MS study of platinum-group and chalcophile elements in base metal sulfide minerals of the Jinchuan Ni–Cu sulfide deposit, NW China

Lie-Meng Chen [a], Xie-Yan Song [a,*], Leonid V. Danyushevsky [b], Yu-Shan Wang [c], Yu-Long Tian [c], Jia-Fei Xiao [a]

[a] State Key Laboratory of Ore Deposit Geochemistry, Institute of Geochemistry, Chinese Academy of Sciences, Guiyang 550002, PR China
[b] ARC Centre of Excellence in Ore Deposits and School of Earth Sciences, University of Tasmania, Private Bag 79, Hobart, Tasmania 7001, Australia
[c] Jinchuan Group Ltd., Jinchang, Gansu 737100, PR China

ARTICLE INFO

Article history:
Received 25 April 2014
Received in revised form 17 July 2014
Accepted 18 July 2014
Available online 31 July 2014

Keywords:
Jinchuan
Platinum-group element
Laser ablation
Base metal sulfide
Magmatic sulfide deposit

ABSTRACT

The paper presents concentrations of the platinum-group and chalcophile elements in the base metal sulfides (BMS) from the Jinchuan Ni–Cu sulfide deposit determined by laser ablation-inductively coupled plasma-mass spectrometry. Mass balance calculations reveal that pentlandite hosts a large proportion of Co, Ni and Pd (>65%), and that pentlandite and pyrrhotite accommodate significant proportions of Re, Os, Ru, Rh, and Ag (~35–90%), whereas chalcopyrite contains a small amount of Ag (~10%) but negligible platinum-group elements. Iridium and Pt are not concentrated in the BMS and mostly occur in As-rich platinum-group minerals. The enrichments of Co, Ni, Re, Os, Ru, and Rh in pentlandite and pyrrhotite, and Cu in chalcopyrite are consistent with the fractionation of sulfide liquid and exsolution of pentlandite and pyrrhotite from the mono-sulfide solid solution (MSS). The Ir-bearing minerals exsolved from the MSS, depleting pentlandite and pyrrhotite in Ir, whereas sperrylite exsolved from the residual sulfide liquid on cooling. Diffusion of Pd from residual sulfide liquid into pentlandite during its exsolution from the MSS and crystallization of Pt-bearing minerals in the residual sulfide liquid resulted in the enrichment of Pd in pentlandite and decoupling between Pd and Pt in the Jinchuan net-textured and massive ores.

1. Introduction

Magmatic sulfide deposits are a result of concentration of sulfide liquid droplets with high concentrations of platinum-group and chalcophile elements (Barnes and Lightfoot, 2005; Naldrett, 2004). The platinum-group elements (PGE) are hosted not only by platinum-group minerals (PGM), but also by base metal sulfide (BMS) minerals. In PGE-rich Ni–Cu ores (e.g., Noril'sk–Talnakh, Barnes et al., 2006, 2008; Cabri et al., 2003) and high-PGE reefs in layered intrusions (the J–M Reef in the Stillwater Complex, Godel and Barnes, 2008; the Merensky Reef and Platreef in the Bushveld Complex, Ballhaus and Sylvester, 2000; Godel et al., 2007; Holwell and McDonald, 2007; Hutchinson and McDonald, 2008), IPGE (Os, Ir, and Ru) and Re are concentrated in pyrrhotite; Ni, Co, Re, IPGE, and Rh are concentrated in pentlandite; whereas Ag, Cd, and Zn are partitioned into chalcopyrite. Platinum minerals are found as inclusions in the BMS and/or hosted at the grain boundaries of the BMS in most magmatic sulfide deposits (Barnes et al., 2008; Dare et al., 2010a, 2010b, 2011, 2014; Godel and Barnes, 2008; Godel et al., 2007; Holwell and McDonald, 2007; Hutchinson and McDonald, 2008; Piña et al., 2012). Palladium is mainly hosted by pentlandite in PGE-rich Ni–Cu ores, whereas in reefs it occurs not only as Pd-bearing PGM, but also can been contained in pentlandite up to 2.8 wt.% (Godel and Barnes, 2008). These observations partly support the model of the mono-sulfide solid solution (MSS) fractionation, which accommodates Re, Rh, and IPGE and exsolves to pentlandite and pyrrhotite at sub-solidus conditions (e.g., Barnes et al., 2006). However, the very low contents of Pt and Pd in the chalcopyrite of all these deposits are surprising, because these metals are commonly believed to concentrate in Cu-rich residual sulfide liquid, which is now represented by chalcopyrite (Cabri, 1973; Ebel and Naldrett, 1996, 1997; Kullerud et al., 1969; Misra and Fleet, 1973). Understanding processes that control the distribution of PGE and chalcophile elements is important for constraining the petrogenesis of sulfide ores and improving the recovery of PGE (e.g., Cabri and Laflamme, 1984; Cabri et al., 2002, 2010).

The giant Jinchuan Ni–Cu sulfide deposit on the southwestern margin of the North China craton contains over 500 million metric tons of sulfide ores grading 1.06 wt.% Ni and 0.7 wt.% Cu (Chai and Naldrett, 1992a, 1992b; Sixth Geological Unit, 1984). Three principal types of

* Corresponding author at: State Key Laboratory of Ore Deposit Geochemistry, Institute of Geochemistry, Chinese Academy of Sciences, 46th Guanshui Road, Guiyang 550002, PR China. Tel./fax: +86 851 5891664.
E-mail address: songxieyan@vip.gyig.ac.cn (X.-Y. Song).

http://dx.doi.org/10.1016/j.oregeorev.2014.07.011
0169-1368/

sulfide mineralization occur in this deposit: disseminated ores, net-textured (+massive) ores, and Cu-rich ores (Jinchuan Nonferrous Metal Corporation, 1997, 2003; Sixth Geological Unit, 1984). The disseminated ores have a positive correlation between Ir and Pd and very high Cu/Pd ratios, indicating that they can represent the original sulfide melts segregated from a PGE-depleted parental magma. The net-textured and massive ores show differentiation between IPGE and PPGE and indicate the fractionation of the sulfide liquid. On the other hand, the Cu-rich ores are characterized by very low IPGE tenors and large Pd/Ir ratios and highly variable Pt tenors, implying that they are formed from the fractionated residual sulfide liquid (Chen et al., 2013; Song et al., 2009; Su et al., 2008). Although the Sixth Geological Unit (1984) has reported that most of Pt and Pd occurred as sperrylite ($PtAs_2$), moncheite ($PtTe_2$), froodite ($PdBi_2$), and michenerite (PdBiTe), with some Pd concentrated in chalcopyrite, Chai et al. (1993) have proposed that over 70% Pd is contained in pentlandite, and Pd minerals were rare. Recently, Prichard et al. (2013) have analyzed the distribution of PGE in PGM in some low-PGE ores, and concluded that the formation of these PGMs is related to hydrothermal remobilization. Thus, the distribution of the PGE and chalcophile elements in the BMS and the processes that have controlled their distribution in the Jinchuan Ni–Cu sulfide deposit are still poorly constrained.

Recent developments in laser ablation-inductively coupled plasma-mass spectrometry (LA-ICP-MS) allow us to determine the PGE and chalcophile elements in the BMS in situ. This technique is a multi-elemental analytical method with low detection limits and invisible damage for samples. It has been successful to determinate a full suite of trace elements in BMS in magmatic sulfide ore deposits. In the present work, we have measured the concentrations of the PGE, Ni, Co, Re, Cu, Ag, and As in the BMS minerals (pyrrhotite, pentlandite, and chalcopyrite) of the Jinchuan deposit. The objectives of this study are: a) to examine whether these elements are located in the BMS, b) to investigate what proportions of these elements are hosted in specific BMS, and c) to estimate what processes play a role in controlling the distribution of these elements in the BMS.

2. Geology of the Jinchuan deposit

The Jinchuan Ni–Cu deposit is hosted by a Neoproterozoic ultramafic intrusion (827 ± 8 Ma, U–Pb SHRIMP zircons, Li et al., 2005; 831.8 ± 0.6 Ma U–Pb ID-TIMS zircons, Zhang et al., 2010) within the northwest-striking Longshoushan Terrane. The Longshoushan Terrane is situated in the southwestern margin of the North China Craton, and is composed of Paleoproterozoic and Mesoproterozoic metamorphic units unconformably overlain by Neoproterozoic and Paleozoic conglomerates, sandstones, and limestones (Fig. 1a; Lehmann et al., 2007; Sixth Geological Unit, 1984; Song et al., 2006; Tang and Li, 1995). The Jinchuan intrusion (~6500 m long and from ~20 m to >500 m wide) intruded into gneisses, schists, marbles and granites of the Paleoproterozoic formation as a dyke-like body (Fig. 1b; Tang and Li, 1995). The elongated body is divided into four segments by a series of NE-trending strike–slip faults F_8, F_{16-1}, and F_{23}, referring as Segments III, I, II and IV from west to east (Fig. 1b). The Segments III and I comprise coarse-grained sulfide-dunite and lherzolite in the Lower unit and fine-grained dunite, lherzolite to minor pyroxenite in the Upper unit (Chen et al., 2009a, 2009b, 2013; Song et al., 2012). On the other hand, Segments II and IV are composed of medium-coarse grained sulfide-dunite and lherzolite (Sixth Geological Unit, 1984; Song et al., 2009). Three largest ore bodies (named No. 1, No. 2 and No. 24) contain >85% of metal reserves of the deposit. The No. 1 and No. 2 ore bodies occur in the western and eastern portions of Segment II, respectively (Fig. 1b). Recently, some individual small sulfide ore bodies have been found in the Proterozoic metamorphic rocks beneath the main intrusion (Jinchuan Nonferrous Metal Corporation, 1997, 2003).

The tabular-shaped No. 24 ore body occurs in the Lower unit of Segments I and III. It is sub-parallel to the wall of the intrusion and is ~1300 m long and ~20–70 m wide, and dips to depths of ~300–500 m southwestwards. The ore body commonly occurs above the basal pyroxenite but may be in contact with the footwall metamorphic rocks where the basal pyroxenite is absent (Sixth Geological Unit, 1984). The main sulfide mineralization of the No. 24 ore body is net-textured (and minor massive), disseminated, and Cu-rich sulfides (Chen et al., 2013; Sixth Geological Unit, 1984).

3. Sulfide mineralogy and textures

Because the sulfide ores in the No. 24 ore body are enriched in PGE compared to ore bodies No. 1 and No. 2 (Chen et al., 2013; Song et al., 2006, 2009; Su et al., 2008), we selected two representative disseminated ores, three net-textured and massive ores from the No. 24 ore body for analysis in this study. These samples are described in detail in Chen et al. (2013) and summarized below briefly.

The disseminated ores contain <15 modal% of BMS (1–8% pyrrhotite, 1–5% pentlandite, and 1–3% chalcopyrite), which are randomly distributed between olivine and clinopyroxene grains (Fig. 2a). The net-textured ores are composed of 15–40% sulfides and 60–85% rounded olivine crystals (Fig. 2b). The net-textured ores have significantly low proportions of chalcopyrite (1–4%) relative to pentlandite (4–10%). Pyrrhotite is a predominant sulfide (10–30%). Pentlandite forms subhedral crystals (0.2–2 mm diameter) and is enclosed by anhedral/subhedral pyrrhotite, or forms aggregates around, or flames within, pyrrhotite (Fig. 2b). Chalcopyrite usually occurs as anhedral assemblages disseminated within the other sulfides or as very minor veinlets which crosscut silicates. The massive ores are commonly present within small fractures and occurs as aggregates or irregular or lenticular veins. The massive ores contain >70% sulfides, including pyrrhotite (40–60%), pentlandite (10–20%) and minor chalcopyrite (1–7%) (Fig. 2c). In contrast, the Cu-rich ores are remarked by relatively high proportions of chalcopyrite (2–14% chalcopyrite, 5–15% pyrrhotite, and 1–6% pentlandite; Fig. 2d).

More than ten different types of PGMs have been identified at Jinchuan. The predominant PGM is euhedral sperrylite ($PtAs_2$) (<0.1 mm in diameter), which occurs either at the contacts of chalcopyrite and pentlandite, or within chalcopyrite. In addition to sperrylite, other PGMs include moncheite ($PtTe_2$), froodite ($PdBi_2$), palladium melonite [(Ni,Pd,Pt)(Te,Bi)$_2$], michenerite (PdBiTe), sudburyite [(Pt,Pd)Sd], and irarsite (IrAsS) (Chai and Naldrett, 1992a; Sixth Geological Unit, 1984; Su et al., 2008; Yang et al., 2006). Moreover, some small grains of Bi–Te compounds in the Cu-rich ores are enclosed by the BMS (Fig. 2d).

4. Analytical methods

The compositions of BMS were measured for major elements (Fe, Ni, Cu, Co, and S) using an EPMA-1600 electron microprobe at the State Key Laboratory of Ore Deposit Geochemistry (SKLODG), Institute of Geochemistry, Chinese Academy of Sciences. Operating conditions were an accelerating voltage of 25 kV, a beam current of 10 nA, and a beam diameter of 5–10 μm. The natural sulfides (marcasite (FeS_2) for Fe and S, pentlandite ($(Fe, Ni)_9S_8$) for Ni, and skutterudite ($(Co, Ni)As_3$) for Co) and synthetic mineral (cuprite (Cu_2O) for Cu) were used as standards. The analytical results are summarized in Table 1.

The contents of platinum-group and chalcophile elements in the BMS were analyzed by LA-ICP-MS at CODES, University of Tasmania, using an Agilent 7500cs quadrupole ICP-MS coupled to a New Wave UP213 Nd:YAG solid state laser ablation system. The following analytical parameters and conditions were used: laser beam diameter of 40–80 μm, depending on the size of grains; laser beam fluence of ~4–5 J/cm^2 at the sample; laser pulse rate of 5 Hz; ablation occurred in the atmosphere of pure He flowing at a rate of 0.8 l/min; immediately past the ablation point within the cell, He carrier gas was mixed with Ar (0.85 l/min) for improved efficiency of aerosol transport; the ICP-MS instrument was optimized to maximize sensitivity on mid- to high-mass

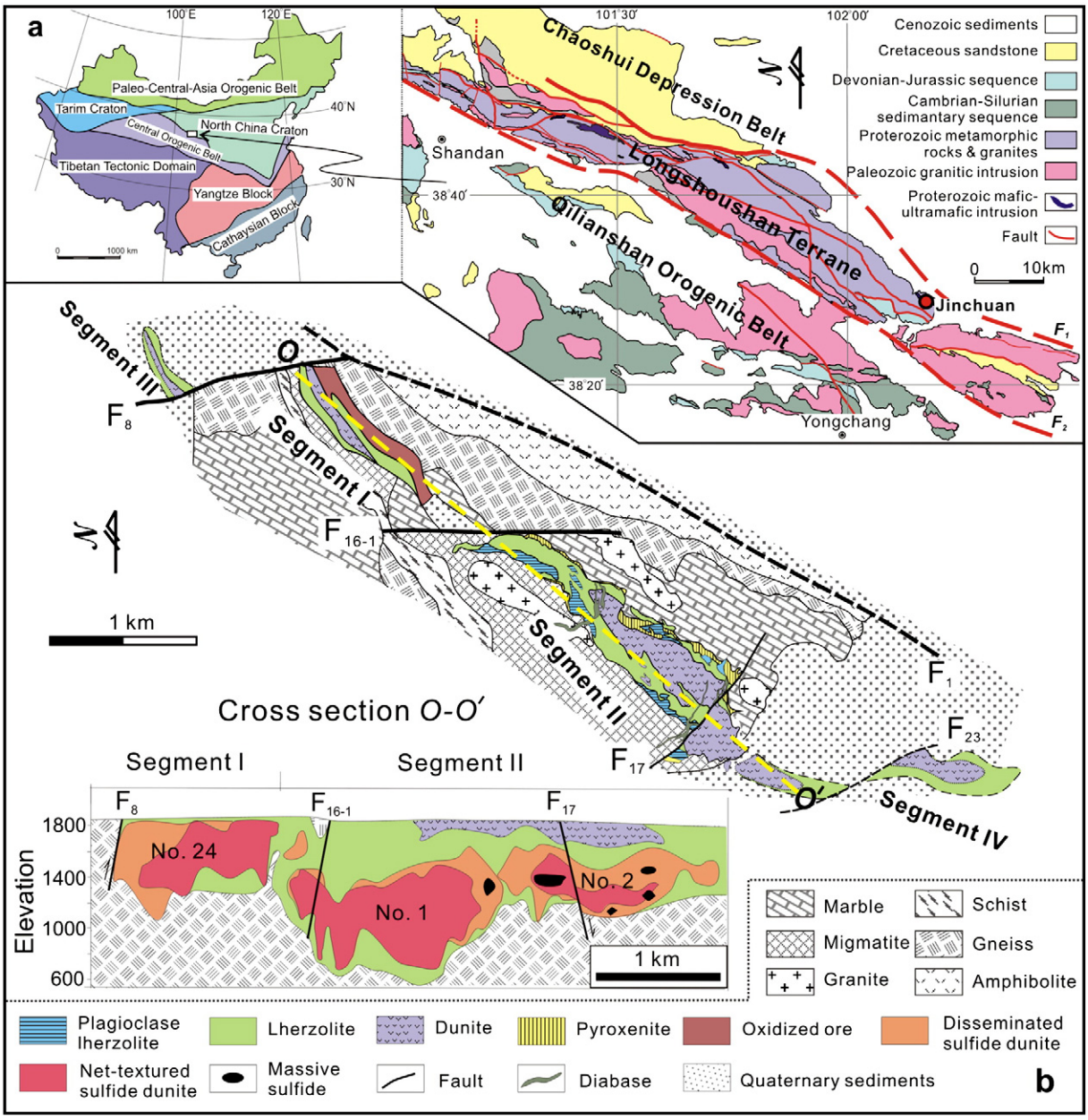

Fig. 1. (a) The main tectonic units of China, and the location of the Jinchuan intrusion at the southwestern margin of the North China Craton. (b) Simplified geological map and a cross section of the Jinchuan intrusion, showing the distribution of rocks and the largest ore bodies.
Modified after Sixth Geological Unit (1984) and Song et al. (2009, 2012).

isotopes (in the range 80–240 amu); production of molecular oxide species (i.e., $^{232}Th^{16}O^{+}/^{232}Th^{+}$) and doubly-charged ion species (i.e., $^{140}Ce^{++}/^{140}Ce^{+}$) was maintained at levels below 0.2%. The rate of Co, Ni, Cu and Zn argide interference production on light PGE (Ru, Rh, Pd) was assessed by ablating pure metals (Guillong et al., 2011), and corresponding corrections were introduced to the signal of light PGE recorded during each analyses.

The following isotopes where measured: ^{57}Fe, ^{59}Co, ^{60}Ni, ^{65}Cu, ^{66}Zn, ^{75}As, ^{82}Se, ^{99}Ru, ^{101}Ru, ^{103}Rh, ^{105}Pd, ^{106}Pd, ^{107}Ag, ^{111}Cd, ^{121}Sb, ^{125}Te, ^{185}Re, ^{189}Os, ^{193}Ir, ^{195}Pt, ^{197}Au, ^{208}Pb, and ^{209}Bi. Each analysis was performed in the time-resolved mode which involves sequential peak hopping through the mass spectrum. The total acquisition time for each analysis was 90 s, comprising a 30 second measurement of the background (laser off) and a 60 second analysis with the laser on.

Data reduction was undertaken according to standard methods (Longerich et al., 1996), using Ni as the internal standard element for the quantification of PGE and Au, and Fe for all other elements. Two primary calibration standards were used: NiS_3 (Gilbert et al., 2013) was used for the quantification of PGE and Au, and STDGL2b2 (Danyushevsky et al., 2003, 2011) was used for the quantification of all other elements. Both standards were analyzed twice every 1–1.5 h to monitor drift in sensitivities. Linear drift corrections were applied between each set of standard analyses. The concentrations of Ni in pyrrhotite and chalcopyrite in each analysis were determined using Fe as the internal standard, and the values obtained were used as the internal standard for the quantification of PGE and Au. Given the very low abundances of Cd in the analyzed minerals, the isobaric interference of ^{106}Cd on ^{106}Pd was negligible. Hence, the ^{106}Pd was used to quantify Pd concentration. A comparison of Pd concentrations determined using ^{105}Pd and ^{106}Pd was used to assess the appropriateness of ^{65}Cu argide interference corrections in high-Cu minerals. This is particularly important as the single ^{103}Rh isotope is subject to argide interference

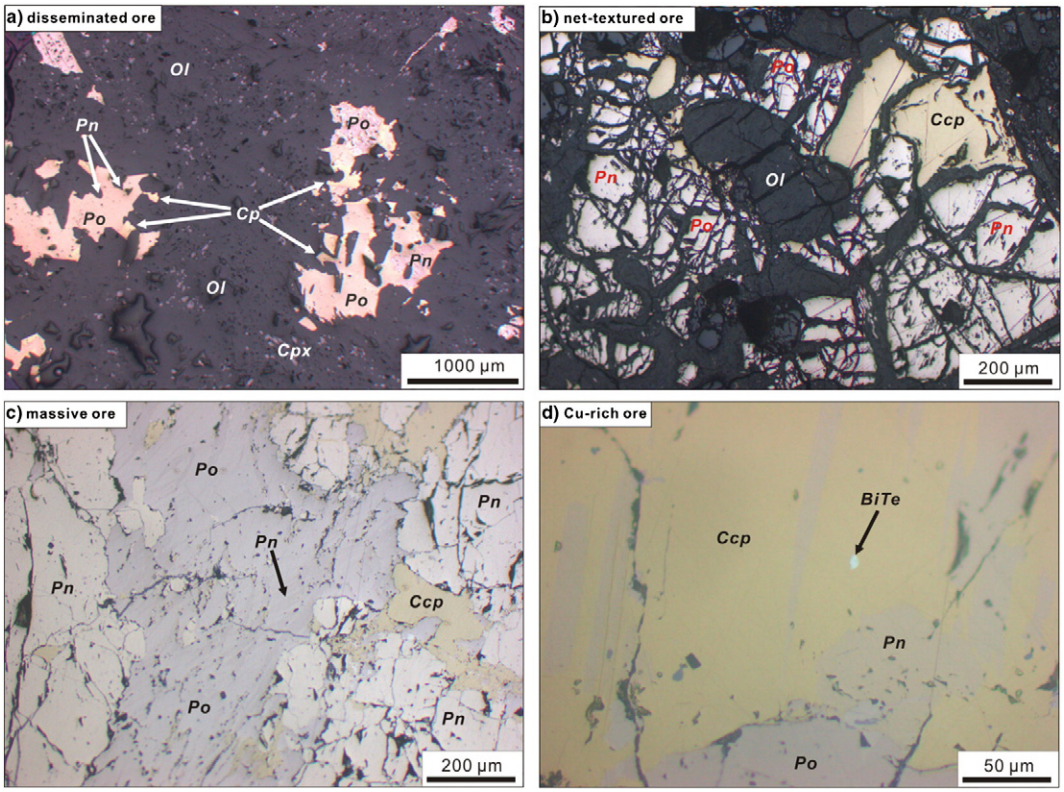

Fig. 2. Microphotographs of sulfide textures of the Jinchuan Ni–Cu sulfide deposit. Ol = olivine; Cpx = clinopyroxene; Pn = pentlandite; Po = pyrrhotite; Ccp = chalcopyrite.

from ^{63}Cu. Analytical accuracy of this study was expected to be better than 20%.

5. Results

5.1. Platinum-group and chalcophile elements in BMS

Concentrations of platinum-group and chalcophile elements in the BMS are listed in Table 2. The complete measured concentrations, detection limits, and analytical precisions can be found in Electronic Appendix A.

5.1.1. Nickel, palladium, and cobalt

Palladium is the most abundant PGE detected in BMS minerals. It is largely partitioned into pentlandite in both disseminated and net-textured and massive ores (from 1750 to 20,600 ppb, with one exception of 170 ppb) and is relatively low in pyrrhotite (<700 ppb, Table 2). Chalcopyrite contains the lowest Pd contents at <100 ppb. Pentlandite and pyrrhotite from the net-textured and massive ores have higher Pd concentrations than those from the disseminated ores (Table 2, Fig. 3a). When all sulfide minerals are considered together, a good correlation between Pd and Ni is observed, demonstrating that Pd is preferentially partitioned into pentlandite (Fig. 3a). In general, the Pd contents of pentlandite are positively correlated to those of the

Table 1
Average contents of major elements in the BMS minerals of the Jinchuan deposit.

Sample no.	Ore type	Mineral	N	S	Fe	Co	Ni	Cu	Total
				wt.%	wt.%	wt.%	wt.%	wt.%	wt.%
JC06-238	Disseminated ore	Pentlandite	3	32.79	27.55	1.75	37.26	0.25	99.59
		Pyrrhotite	10	40.39	59.23	0.04	0.26	0.04	99.96
		Chalcopyrite	4	34.75	31.37	0.00	0.01	33.23	99.37
JC06-226	Disseminated ore	Pentlandite	2	41.73	24.77	1.39	30.04	0.01	97.95
		Pyrrhotite	3	51.22	44.61	0.00	1.31	0.02	97.16
		Chalcopyrite	3	34.82	29.57	0.02	0.36	33.87	98.63
JC06-802	Net-textured ore	Pentlandite	4	32.93	28.80	2.52	35.36	0.03	99.64
		Pyrrhotite	4	45.11	49.07	3.19	0.54	0.09	97.99
		Chalcopyrite	4	34.79	29.60	0.00	0.01	34.71	99.11
JC06-806	Massive ore	Pentlandite	11	31.40	28.80	1.89	36.14	0.01	98.24
		Pyrrhotite	8	40.11	58.24	0.00	0.58	0.01	98.94
		Chalcopyrite	7	34.46	29.67	0.00	0.05	34.85	99.03
GJ08-58-11	Massive ore	Pentlandite	3	41.58	19.70	0.83	36.76	0.36	99.23
		Pyrrhotite	12	52.98	44.99	0.68	0.45	0.51	99.62
		Chalcopyrite	5	34.80	29.95	0.00	0.03	34.55	99.33

N: number of grains analyzed.

Table 2
Concentrations of the platnium-group and chalcophile elements of the BMS minerals by LA-ICP-MS analysis.

Sample No.	Ore type	Grain	Co	Ni	Re	Os	Ir	Ru	Rh	Pt	Pd[a]	Pd[b]	Au	Cu	Ag	Cd	Zn	As	Se	Te	Bi
			ppm	wt.%	ppb	ppb	ppb	ppb	ppb	ppb	ppb	ppb	ppb	wt.%	ppm	ppm	ppm	ppm	ppm	ppm	ppm
Pentlandite																					
JC06-238	Disseminated ore	1	7996	24.6	33.3	317	<13	<33	<16	<25	<62	171	12.6	3.92	105	0.61	5.21	0.77	203	0.47	1.34
JC06-226	Disseminated ore	1	7362	25.7	17.6	87.7	<4	270	<8	<9	2819	3072	<9	1.17	25.4	<0.34	8.07	4.91	272	10.9	0.31
		2	6534	21.2	13.5	164	<7	282	<40	<16	2352	2717	<8	2.85	20.1	<0.73	14.6	0.40	209	0.37	1.85
		3	6230	22.0	69.4	110	<5	354	69.9	<13	1662	1750	<8	1.21	20.2	<0.55	17.6	17.6	196	15.4	1.47
		4	7372	27.6	231	369	5.9	495	291	<12	2229	2521	<8	1.21	28.5	<0.38	24.1	121	359	183	1.04
JC06-802	Net-textured ore	1	12,485	36.9	<10	<37	<9	446	<15	<27	10,277	10,408	13.1	0.042	11.8	1.16	57.1	<0.84	133	7.19	0.77
		2	13,880	41.1	<11	<23	<7	277	43.1	<24	12,583	12,464	40.0	0.011	25.4	<0.97	5.93	0.96	151	32.5	0.45
JC06-806	Massive ore	1	10,044	38.2	138	229	25.5	1001	<19	<20	3668	3695	<14	0.001	15.4	<0.9	16.7	2.24	111	6.09	0.32
		2	10,004	39.3	169	3142	14.6	2002	74.1	<37	3025	3005	<21	0.002	10.4	<0.95	1.26	3.48	92.0	18.5	0.47
		3	9766	42.5	303	292	18.5	715	71.3	<33	3687	3745	12.0	0.001	4.2	<1.08	<0.56	2.88	124	10.4	0.07
		4	10,290	36.5	191	1421	9.5	1230	51.5	<24	3164	3116	20.1	0.001	8.3	<0.80	<0.7	2.34	106	4.35	0.11
		5	10,203	35.9	346	1822	429	1421	1526	33.3	4245	4335	<24	0.087	10.1	<0.89	<0.65	28.1	114	10.3	0.14
GJ08-58-11	Massive ore	1	3411	39.8	2673	665	32.9	845	178	<17	16,504	16,249	26.7	0.71	28.0	1.51	9.06	16.1	300.8	42.6	3.38
		2	3104	37.6	256	1732	19.9	2054	1126	<19	13,775	13,541	28.6	0.97	29.7	1.02	7.84	14.2	360.4	63.2	2.34
		3	3439	39.7	15.4	419	14.1	808	406	<9	16,332	16,863	13.1	0.69	28.1	1.22	2.06	6.83	294.6	40.9	1.18
		4	3496	44.4	15.3	421	21.1	716	235	<19	15,049	15,092	18.1	0.80	36.9	1.18	2.20	6.86	362.5	50.1	0.35
		5	4107	50.9	3024	4550	167	4269	1347	47.7	19,116	19,465	37.0	0.78	32.9	1.49	3.17	7.94	460.6	71.1	2.59
		6	3999	49.5	249	1113	241	912	1150	100	20,197	20,627	39.3	1.06	36.4	1.95	13.4	12.1	458.8	79.2	1.94
		7	3189	39.9	6001	1576	970	1345	934	264	13,542	14,030	58.7	1.47	32.6	1.73	12.2	10.2	318.3	39.0	3.97
Pyrrhotite																					
JC06-238	Disseminated ore	1	5.94	0.11	141	441	<11	345	<18	<9	37	<46	<14	0.0002	4.53	0.75	0.39	1.05	236	0.53	0.59
		2	6.53	0.10	197	444	<9	349	<18	<32	<52	<43	<22	0.0001	2.27	0.48	0.26	<0.83	222	0.22	0.52
		3	7.56	0.06	464	471	<8	312	<14	<20	<41	<50	<12	0.0001	4.85	0.16	1.16	<0.65	220	0.84	0.80
JC06-226	Disseminated ore	1	330	2.56	164	383	<4	226	<10	<17	<27	<27	<8	0.016	3.64	<0.50	3.82	58.0	346	0.02	0.71
		2	212	1.91	75.6	385	<4	212	<8	<14	<27	<24	<9	0.011	3.40	0.32	12.5	22.6	364	0.27	0.59
JC06-806	Massive ore	1	212	0.96	342	1074	9.07	1046	<19	<19	56	50.1	17.8	0.14	3.10	<0.90	0.62	0.14	109	0.32	1.31
		2	833	3.14	313	788	38.5	824	<20	<20	130	305	30.0	0.65	5.71	0.53	1.48	0.28	111	0.54	1.98
		3	295	1.26	559	579	5.30	1046	<17	<23	83	65.6	37.5	0.02	5.08	<0.89	0.59	<0.78	107	0.14	1.01
		4	265	1.04	210	824	<8	722	<23	<20	<41	61.2	35.6	0.87	5.37	0.57	5.39	<0.82	105	0.15	3.19
		5	54.8	0.56	235	1433	1791	1097	2801	90.5	284	275	67.8	0.01	2.71	<0.81	0.89	27.4	113	0.48	0.66
GJ08-58-11	Massive ore	1	1961	2.66	9.58	1200	35.6	848	27.0	10.1	<32	67.1	43.0	2.27	14.6	4.33	82.6	11.0	310	3.84	20.7
		2	11,665	2.07	1870	1322	75.5	1025	340	16.1	479	730	428	1.69	16.4	11.8	383	26.0	324	154	133
Chalcopyrite																					
JC06-238	Disseminated ore	1	0.13	0.002	<9	28.4	<13	85.2	<25	<31	<90	<62	<19	31.7	52.9	3.13	293	<1.01	213.0	17.50	2.64
JC06-802	Net-textured ore	1	27	0.04	<10	<35	<8	85.8	<19	<28	<57	46.6	36.9	31.6	17.9	10.7	849	<0.83	155.7	5.78	0.89
JC06-806	Massive ore	1	298	0.26	295	494	<10	220	<13	<26	37	41.2	32.4	28.4	7.71	4.63	460	0.80	93.6	0.31	4.01

<: blow the detection limit.
[a] Isotope of Pd is 105.
[b] Isotope of Pd is 106.

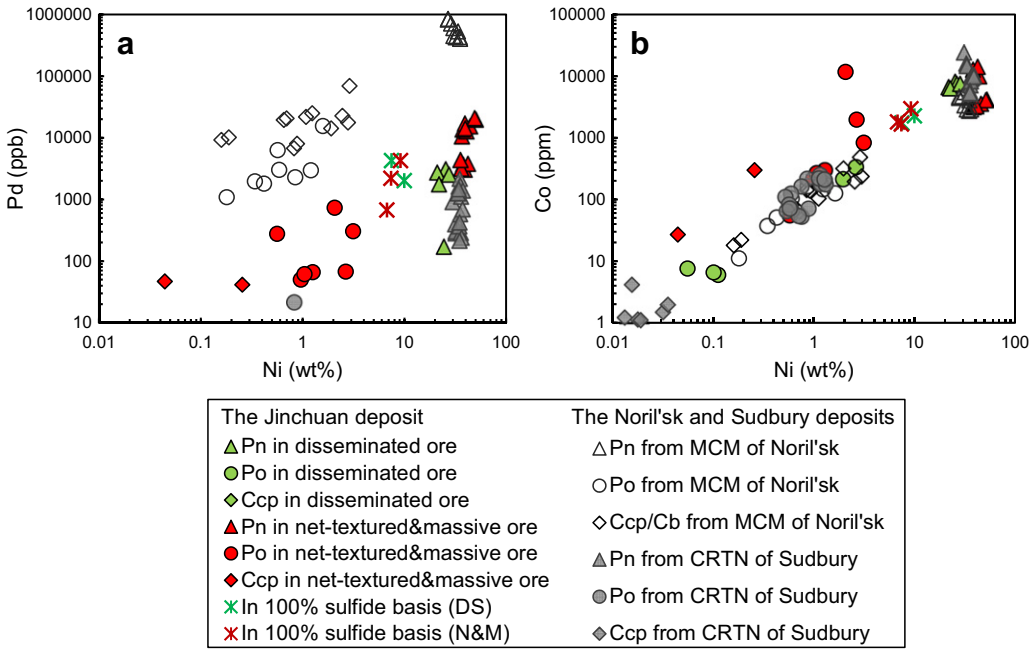

Fig. 3. Binary variation diagrams of Ni versus (a) Pd, and (b) Co of various base-metal sulfide minerals and whole rocks, the good correlation between Ni and these elements, indicating that they are largely contained in pentlandite. DS = disseminated ore; N&M = net-textured and massive ore; MCM = the Medvezhiy Creek Mine, Noril'sk, data from Barnes et al. (2006, 2008); CRTN = the Creighton deposit, Sudbury, data from Dare et al. (2010a).

bulk samples (Table 3, Fig. 3a). These values are in agreement with Chai et al. (1993) who reported that Pd concentrations for pentlandite, pyrrhotite and chalcopyrite are 120–6360 ppb, 6–800 ppb and 10–20 ppb, respectively. These results are somewhat higher than those analyzed by Prichard et al. (2013; 40 to 4200 ppb in pentlandite, <150 to 660 ppb in pyrrhotite, and <150 ppb in chalcopyrite).

Similar to Pd, Co is also primarily contained in pentlandite (3100 to 13,900 ppm), followed by pyrrhotite (6 to 2000 ppm, up to 11,700 ppm in one grain), and chalcopyrite (<0.2 to 300 ppm). Furthermore, the flames of pentlandite (grains 2 and 7 in GJ08-58-11) contain lower Co and Pd concentrations than the co-existing granular pentlandite grains (grains 1, 3 to 6 in GJ08-58-11, Table 2). A strong positive correlation between Co and Ni is observed when all sulfides are compared (Fig. 3b).

The trends of the distributions of Pd, Co, and Ni in the Jinchuan BMS are similar to those from sulfide droplets of the Medvezhiy Creek Mine, Noril'sk (Barnes et al., 2006, 2008) and those from the Creighton deposit, Sudbury (Dare et al., 2010a) (Fig. 3). However, the Jinchuan BMS contain much less Pd relative to those in the Medvezhiy Creek Mine, Noril'sk (200,000–1,200,000 ppb in pentlandite, 1000–10,000 ppb in pyrrhotite, and 4000–30,000 ppb in chalcopyrite/cubanite), but higher than the Creighton deposit, Sudbury (200–2100 ppb in pentlandite, <25 ppb in pyrrhotite, and <35 ppb in chalcopyrite).

5.1.2. Copper, platinum, silver and arsenic

Only minor Pt is partitioned into BMS. Platinum contents vary between <10 and 260 ppb in pentlandite and between <10 and 90 ppb in pyrrhotite. All chalcopyrite grains have Pt values lower than the detection limits (~30 ppb). These are consistent with data reported by Chai et al. (1993) and Prichard et al. (2013). Platinum does not display any correlation with Cu, As or other metals in BMS minerals. It is interesting, however, platinum displays a clear correlation with As and Cu in bulk samples recalculated to 100% sulfide (Fig. 4a–b).

Silver, in contrast to Pt, shows good positive correlations with Cu contents in both BMS and bulk samples (Fig. 4c). Chalcopyrite contains

Table 3
Whole rock concentrations of the platnium-group and chalcophile elements and recalculation to 100% sulfide of the samples.

Sample	Ore type	S	Co	Ni	Cu	Re	Os[a]	Ir	Ru	Rh	Pt	Pd	Au	Ag	Cd	Zn	As	Bi
		wt.%	ppm	wt.%	wt.%	ppb	ppb	ppb	ppb	ppb	ppb	ppb	ppb	ppm	ppm	ppm	ppm	ppm
Whole rock concentrations of S and metals[b]																		
JC06-238	Disseminated ore	1.83	167	0.48	0.56	12.4	6.78	5.22	9.27	4.73	854	213	193	3.2	1.1	170	117	14
JC06-226	Disseminated ore	4.27	344	1.27	0.75	26.0	15.4	20.0	15.3	7.31	276	234	70	4.9	<0.5	130	13	4.0
JC06-802	Net-textured ore	20.9	1005	4.23	1.97	253	62.3	238.0	91.7	78.7	102.1	1216	25	9.6	0.6	115	3.9	1.5
JC06-806	Massive ore	32.7	1630	5.94	1.50	568	512	570	537	168	59.64	579	36	4.3	0.6	31	4.8	3.4
GJ08-58-11	Massive ore	32.0	2600	7.96	1.53	465	712	1880	908	489	879	3618	57	11.5	2.3	63	10	11
Recalculation[c] to 100% sulfides by assuming for 0.1 wt.% Ni, 80 ppm Co, and 10 ppm Zn in the silicate minerals[c]																		
JC06-238	Disseminated ore	36.3	1726	7.54	11.1	246	134	104	184	93.9	16,930	4234	3828	63.5	21.8	3174	2321	278
JC06-226	Disseminated ore	36.7	2267	10.05	6.44	223	133	172	132	62.8	2370	2013	601	42.1	–	1030	112	34.4
JC06-802	Net-textured ore	37.7	1668	7.45	3.55	457	112	429	165	142	184	2193	45.1	17.3	1.08	189	7.0	2.7
JC06-806	Massive ore	38.0	1802	6.8	1.74	661	595	662	625	196	69.3	674	41.9	5.0	0.70	24.4	5.6	3.9
GJ08-58-11	Massive ore	37.6	2960	9.23	1.79	546	836	2208	1066	574	1033	4249	67.0	13.5	2.70	62.3	11.7	12.9

[a] The Os contents were obtained by isotope dilution (ID)-ICP-MS using an improved Carius tube technique (Qi et al., 2007) at SKLODG.
[b] Data of the whole rock concentrations are from Chen et al. (2013) except for Os.
[c] Using $C_{(100\%\ sul)} = C_{wr} * 100 / (2.527 * S + 0.3408 * Cu + 0.4715 * Ni)$ (Barnes and Lightfoot, 2005) to recalculate, where C_{wr} = concentration of the element in the whole rock; S, Cu, and Ni = concentration of these elements in the whole rock (Table 1), in wt.%; –: unavailable values due to blow the detection limit in the values.

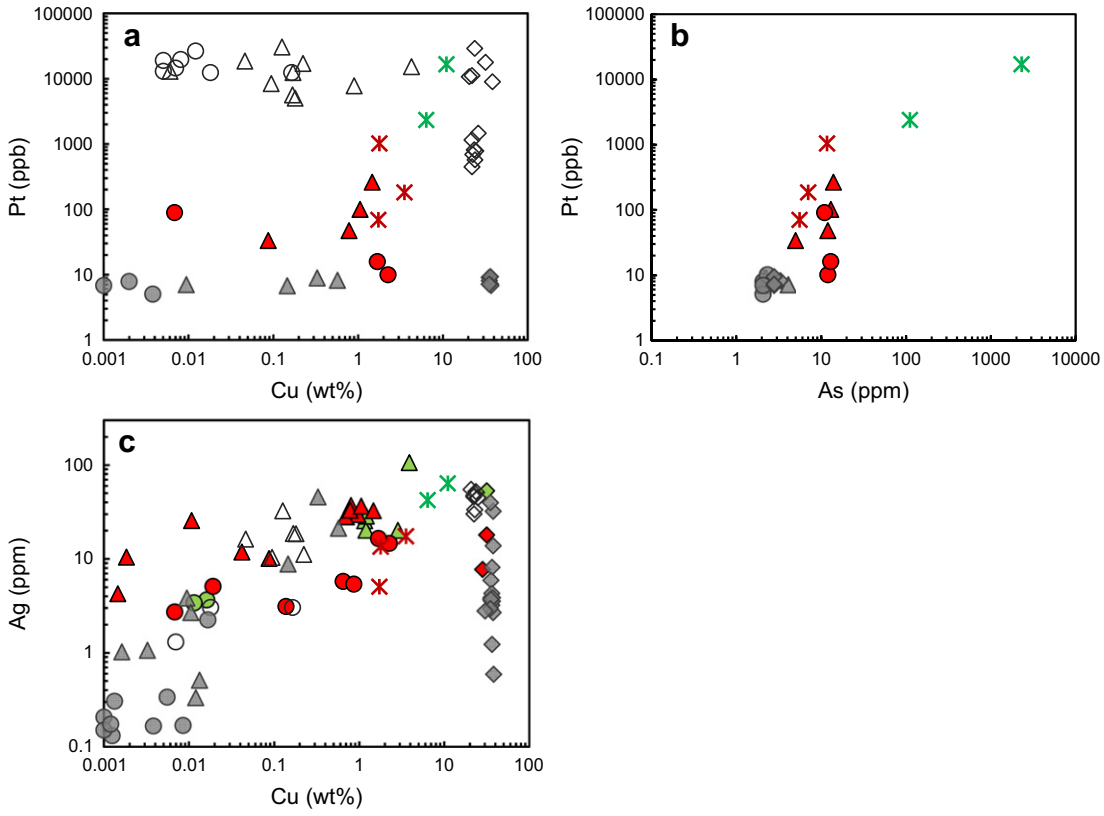

Fig. 4. Binary variation diagrams of (a) Cu vs. Pt, (b) As vs. Pt, and (c) Cu vs. Ag. The positive correlations of Cu vs. Ag imply that Ag is partitioned into chalcopyrite; on the other hand, Pt does not correlate with Cu, and As in BMS, but shows a good correlation in whole rock. The symbols are the same as Fig. 3.

the majority Ag (8–50 ppm), followed by pentlandite (4–40 ppm Ag, except one grain of 105 ppm) and pyrrhotite (2–20 ppm Ag). Both pentlandite and pyrrhotite contain approximately equal As contents, varying from 0.4 to 120 ppm and 0.1 to 60 ppm, respectively, whereas chalcopyrite hosts the lowest As concentrations (<1 ppm) (Table 2, Fig. 4b).

The considerably low Pt contents in all BMS minerals were also found in other studies, such as those of the Creighton deposit, Sudbury (<10 ppb, Dare et al., 2010a), which are much lower than those of the Medvezhiy Creek Mine, Noril'sk (>500 ppb; Barnes et al., 2006, 2008). On the other hand, BMS in both Jinchuan and the Medvezhiy Creek Mine in Noril'sk have similar contents of Ag, which are higher than those of the Creighton deposit in Sudbury (Barnes et al., 2006, 2008; Dare et al., 2010a). The correlation between Ag and Cu in Jinchuan are similar to those from the Medvezhiy Creek Mine and the Creighton deposits (Fig. 4c–d).

5.1.3. Ruthenium, osmium, iridium, rhodium, and rhenium

Ruthenium and Os contents in both pentlandite and pyrrhotite are similar (200–4300 ppb Ru with one grain <30 ppb, and 90–4600 ppb Os with two exceptions <40 ppb); these values are generally higher than those in chalcopyrite (<250 ppb Ru, and <35 ppb Os except one grain of 500 ppb). Concentrations of Ir of pentlandite (<5 to 1000 ppb) are slightly greater relative to pyrrhotite (5–40 ppb, with one grain exception up to 1800 ppb), and those of chalcopyrite are below detection limits (8–15 ppb). Rhodium contents are higher in pentlandite (40–1500 ppb, with four grains below 20 ppb) and pyrrhotite (30–300 ppb, with one grain up to 2800 ppb), than in chalcopyrite (below detection limits of 10–30 ppb in all analyses) (Table 2). The concentrations of Ru, Os, Ir and Rh in pentlandite and pyrrhotite from the net-textured and massive ores are greater than those from the disseminated ores (Table 2, Fig. 5a–c). Both Os and Rh correlate positively with Ru (Fig. 5a–b). In contrast, no correlations between Ir and Ru are observed (Fig. 5c).

Rhenium concentrations vary significantly in all BMS. Values in pentlandite (10 to 6000 ppb) are generally higher than in pyrrhotite (10 to 2000 ppb) and chalcopyrite (<10 ppb, except one grain 300 ppb that has high Os content) (Table 2). Similar to Ru, Os, Ir and Rh, the contents of Re in the net-textured and massive ores are higher than those in the disseminated ores (Table 2, Fig. 5d).

The trends of the distributions of Os, Rh and Ru in the BMS are similar to those from the Medvezhiy Creek Mine in Noril'sk (Barnes et al., 2006, 2008) and the Creighton deposit in Sudbury (Dare et al., 2010a) (Fig. 5a–b). On the other hand, the relationships between Ir, Re and Ru in the BMS are different from those of the Medvezhiy Creek Mine and the Creighton deposit (Fig. 5c–d).

5.2. Mantle-normalized metal patterns

In primitive mantle-normalized diagrams, pentlandite shows a very uneven pattern, with enriched Re, Ru, Rh and Pd contents (which are also higher than in the bulk samples), and clearly negative anomalies of Ir and Pt (Fig. 6a). Pyrrhotite patterns are characterized by Re, Ru, and Rh enrichments, and significantly negative Ir, and Pt anomalies and large variations in Co (Fig. 6b). As mentioned above, the concentrations of Ir, Rh, and Pt in most chalcopyrite are below detection limits, and thus their patterns are enriched in Re and Ag relative to other metals (Fig. 6c).

The mantle normalized metal patterns for pentlandite, pyrrhotite, and chalcopyrite of the Jinchuan Ni–Cu sulfide deposit are similar to those of the Creighton deposit, Sudbury (Dare et al., 2010a), but are different from those of the Medvezhiy Creek Mine, Noril'sk (Barnes et al., 2006, 2008) (Fig. 6).

6. Discussion

Compositions of platinum-group and chalcophile elements are taken to indicate that the Jinchuan sulfides had experienced extensive fractionation of the immiscible sulfide liquid (Chai and Naldrett, 1992a; Chen et al., 2013; Song et al., 2006, 2009; Su et al., 2008). The present study permits us to evaluate the precise location of the PGE and chalcophile elements in the BMS, the timing and mechanism of the observed decoupling of Pd and Pt, and the mechanisms and processes controlling the distributions of PGE in Jinchuan.

6.1. Mass balance calculations of PGE and chalcophile elements

As shown on the Figs. 3, 4, and 5, concentrations of some PGE and chalcophile elements (e.g., Pd, Os, Ru, Rh, Co, and Ag) in 100% sulfide bulk samples plot within the BMS mineral trends, suggesting that these metals are predominantly hosted in BMS. On the other hand, Ir, and Pt tenors in 100% sulfide bulk samples are above the BMS trends, indicating that there are other phase(s) in addition to BMS that also carry these metals in the samples.

Aiming to quantitatively investigate the percentages of these metals in the BMS, we have calculated the proportion of element i (P^i_{sul}) following the method proposed by Barnes et al. (2006):

$$P_{sul}{}^{i} = \left(F_{sul} \times C_{sul}{}^{i} / C_{WR}{}^{i}\right) \quad (1)$$

where F_{sul} is the weight fraction of the BMS, and C^i_{sul} and C^i_{WR} are the content of the element i in the BMS (Table 2) and in the bulk samples (Table 3). F_{sul} is estimated following the procedure described by Barnes et al. (2006). The Ni contents in silicates are assumed to be 0.1 wt.% and have been removed before the calculation of fractions of pentlandite, pyrrhotite, and chalcopyrite in 100% sulfide as illustrated in the Table 3. Additionally, the compositions of the BMS are from Table 1. Note that some elements are below the detected limits of LA-ICP-MS analysis (i.e., Re, Os, Ru and Rh in some samples; Ir and Pt in most ores), and in these cases the detection limit values were used in calculations. The results of the mass balance calculations are presented in Table 4 and Fig. 7.

The calculations indicate that pentlandite contains a large proportion of Pd in these ores (>65%, mean value of all samples) (Table 4, Fig. 7a). Pyrrhotite contains 5% Pd. Osmium, Ru and Re are accommodated mainly by pyrrhotite (~60% Os, ~40% Ru, and ~30% Re) and, to lesser extent, pentlandite (~30% Os, ~35% Ru, and ~15% Re) (Table 4, Fig. 7a), even though the latter has higher contents of these elements than the former. A moderate proportion of Rh is present in pentlandite (~25%). Pyrrhotite hosts less Rh (<10%) than pentlandite in the BMS. In most samples with one exception (GJ08-58-11), cobalt and Ni are hosted mostly by pentlandite (~70% and ~80%, respectively), and pyrrhotite (~25% and ~10%, respectively) (Table 4, Fig. 7a).

It is surprising that only ~1–5% Ir is hosted by BMS for all samples (Table 4, Fig. 7a), since Ir is expected to have a similar geochemical behavior to Os and Ru. Only a very small portion of Pt (<5%, with one expectation of 30% for JC06-806) present can be accounted for by BMS and it is not preferentially distributed into any mineral (Table 4, Fig. 7a). The observed depletions of Ir and Pt in sulfide minerals indicate that they should occur predominantly as PGM or metal-alloy(s). In addition, copper is mainly hosted by chalcopyrite (~85%), followed by pyrrhotite (~15%) and pentlandite (~5%), whereas silver is equally incorporated into pentlandite (~30%) and pyrrohotite (~30%), followed by chalcopyrite (~10%) (Table 4, Fig. 7a).

The observed large proportions of Co, Ni, Re, Os, Ru, and Pd contained in pentlandite and pyrrhotite in Jinchuan are similar to what is observed in the Medvezhiy Creek, Noril'sk (Barnes et al., 2006,

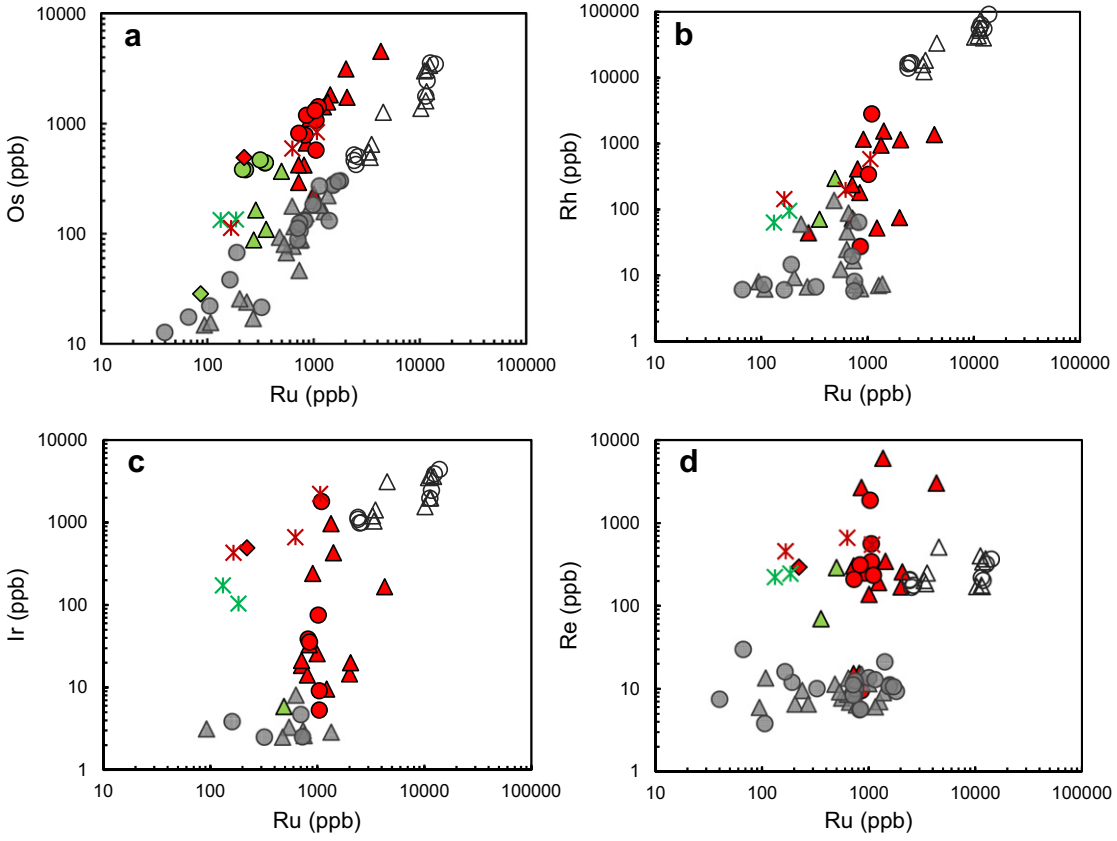

Fig. 5. Binary variation diagrams of Ru versus (a) Os, (b) Rh, (c) Ir, and (d) Re. There are strongly positive correlations of Ru vs. Os and Rh, whereas weak correlations of Ru vs. Ir and Re. The symbols are the same as Fig. 3.

2008), whereas the percentages of Ir and Rh are much lower (Fig. 7b). Compared to the Creighton sulfide deposit, Sudbury (Dare et al., 2010a), BMS minerals in Jinchuan host similar proportions of Os, Ir, Ru, and Pd, but higher proportions of Re, Rh, and Ag (Fig. 7c).

6.2. Role of fractionation of the sulfide liquid

Experimental studies have shown that the sulfide liquid starts to fractionate MSS at temperatures of ~1190 °C. Osmium, Ir, and Ru are compatible elements and enriched in MSS, while Cu, Pt, and Pd are incompatible elements to MSS and are partitioned into the residual sulfide liquid that would crystallize intermediate solid solution (ISS) at temperatures of ~900 °C; the latter later breaks down forming chalcopyrite on cooling (Ballhaus et al., 2001; Fleet et al., 1993, 1996; Kullerud et al., 1969; Li et al., 1996). Nickel is moderately incompatible with MSS at high temperatures (>1150 °C), but becomes generally more compatible at lower temperatures (<1000 °C) (Barnes et al., 1997; Mungall et al., 2005).

Based on the experimental partition coefficients, one would expect that pentlandite and pyrrhotite, which represent the breakdown products of MSS, are enriched in IPGE. Indeed, our LA-ICP-MS results reveal that the distributions of the PGE and other chalcophile elements in Jinchuan BMS are mainly controlled by their partitioning behavior during the fractionation of sulfide liquid and breakdown of MSS. Cobalt, Re, Os, and Ru are concentrated in pyrrhotite and pentlandite of the net-textured and massive ore (Fig. 7a). In addition, pentlandite in the net-textured and massive ores has higher concentrations of these elements than pyrrhotite (Figs. 3, 5), indicating that these metals preferentially partition into pentlandite during MSS breakdown (Ballhaus and Sylvester, 2000; Holwell and McDonald, 2007). Rhodium is also compatible in MSS, however it partitions slightly more into pentlandite than pyrrhotite (Fig. 5b). Thus, we propose that Rh concentrates preferentially into the Ni-rich MSS which forms pentlandite on cooling. The strong correlation between Co and, to a lesser extent, IPGE with Ni indicates that Co is mainly substituting for Ni in pentlandite. On the other hand, the tendencies for Re and IPGE to concentrate in both pyrrhotite and pentlandite suggest that these elements substitute for Fe during MSS breakdown (Barnes et al., 2008).

Chalcopyrite hosts negligible amounts of PGE, consistent with previous studies (e.g., Barnes et al., 2008; Dare et al., 2010a, 2010b, 2011, 2014; Piña et al., 2012). This is because Pt and Pd are incompatible in ISS (Peregoedova, 1998). Instead, chalcopyrite accommodates significant proportions of incompatible elements, such as Cu and Ag (Figs. 4c, 8a), supporting an interpretation that chalcopyrite represents solidification production of the residual Cu-rich liquid.

6.3. Crystallization of PGM

The extremely low proportions of Ir and Pt in Jinchuan BMS indicate that they occur predominantly as PGM (and/or metal-alloys) (Fig. 7). Platinum-group minerals dominantly include Pt-bearing minerals (e.g., sperrylite) and several Pd-bearing minerals (michenerite, sudburyite) at Jinchuan (Chai and Naldrett, 1992a; Prichard et al., 2013; Su et al., 2008; Yang et al., 2006). Mineral separation experiments have indicated that 62–99 wt.% of the amount of Pt in the whole rock can be accounted for by the Pt-bearing minerals (Sixth Geological Unit, 1984). No Ir-bearing mineral has been found in the heavy-mineral separations; however, solution tests have revealed that a large proportion of Ir was not separated successfully, which suggests that it is possibly present as PGM (Chai et al., 1993; Sixth Geological Unit, 1984). Furthermore, multiple anomalies of Ir, Rh, and As in the LA-ICP-MS spectra obtained during the analysis of pentlandite (Fig. 8), together with the results of Prichard et al. (2013), support a speculation that Ir mainly exists as a very fine Ir-bearing sulfur-arsenide enclosed in the BMS (i.e., Ir–Rh–As–S), similar to the irarsite and/or hollingworthite mixture in the Creighton deposit, Sudbury (Dare et al., 2010b).

Euhedral or anhedral PGM crystals with sizes varying from 2 to 100 μm and inclusions of PGM in BMS suggest that they may have crystallized from the sulfide liquid (Prichard et al., 2013). The timing of PGM crystallization varies in different deposits. Discrete PGM may crystallize

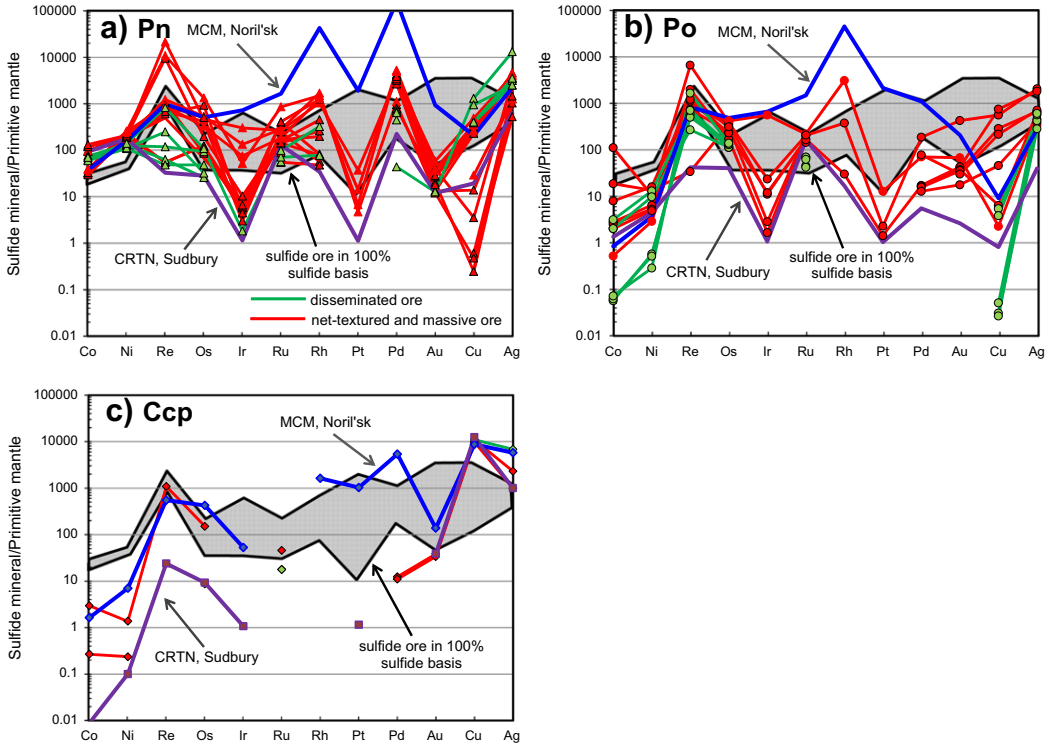

Fig. 6. Mantle normalized metal patterns for (a) pentlandite (Pn), (b) pyrrhotite (Po), and (c) chalcopyrite. Normalization values from McDonough and Sun (1995). Data from the Jinchuan deposit (this study), the Medvezhiy Creek Mine (MCM), Noril'sk (Barnes et al., 2006, 2008), and the Creighton deposit (CRTN), Sudbury (Dare et al., 2010a).

Table 4
Weight percent (%) of each element in each sulfide mineral and weight percent (%) of the element in the sulfide fraction.

Sample no.	Ore type	Mineral	Fraction (%)	Co	Ni	Re	Os	Ir	Ru	Rh	Pt	Pd	Au	Cu	Ag
JC06-238	Disseminated ore	Pn	1.0	48.8	52.2	2.7	46.6	2.5	3.6	3.4	0.03	0.8	0.1	7.0	33.6
		Po	0.7	0.03	0.1	15.4	46.5	1.3	25.8	2.5	0.02	0.2	0.1	0.00	0.9
		Ccp	1.7	0.00	0.01	1.2	6.9	4.2	15.5	8.9	0.1	0.5	0.2	93.0	27.9
		Total BMS	3.4	48.9	52.4	19.3	100.0	8.0	44.9	14.9	0.1	1.5	0.3	100.0	62.3
JC06-226	Disseminated ore	Pn	3.9	77.8	74.0	12.4	33.6	1.1	63.0	54.5	0.2	41.8	0.5	8.4	18.7
		Po	3.7	2.9	6.4	16.9	66.4	0.7	37.0	4.5	0.2	0.2	0.4	0.1	2.6
		Ccp	2.2												
		Total BMS	9.8	80.7	80.4	29.3	100.0	1.8	100.0	59.0	0.4	42.0	0.9	8.4	21.3
JC06-802	Net-textured ore	Pn	11.7	99.0	98.9	0.5	5.6	0.4	46.0	4.3	2.9	99.8	12.4	0.2	22.6
		Po	33.4												
		Ccp	5.7	1.0	1.1	0.2	3.2	0.2	5.3	1.4	1.6	0.2	8.4	90.9	10.6
		Total BMS	50.8	100.0	100.0	0.7	8.8	0.6	51.3	5.7	4.5	100.0	20.8	91.1	33.2
JC06-806	Massive ore	Pn	16.4	85.8	85.7	6.6	29.2	2.9	25.8	34.0	8.1	88.0	8.3	0.2	31.4
		Po	65.0	13.5	14.1	40.7	68.1	1.7	73.0	7.6	22.4	18.2	54.6	18.1	62.0
		Ccp	4.3	0.7	0.2	2.2	2.7	0.1	1.2	0.3	1.9	0.3	3.9	81.5	6.6
		Total BMS	85.8	100.0	100.0	49.6	100.0	4.7	100.0	42.0	32.3	100.0	66.8	99.8	100.0
GJ08-58-11	Massive ore	Pn	21.7	21.7	90.7	49.8	38.8	2.4	37.3	34.0	1.7	95.7	12.0	13.2	52.5
		Po	40.5	78.3	9.3	50.2	61.2	1.2	41.8	15.2	0.6	4.3	30.6	52.5	47.5
		Ccp	4.4												
		Total BMS	66.6	100.0	100.0	100.0	100.0	3.6	79.1	49.2	2.3	100.0	42.6	65.7	100.0
Average		Pn		66.6	80.3	14.4	30.8	1.9	35.2	26.1	2.6	65.2	6.7	5.8	31.8
		Po		23.7	7.5	30.8	60.6	1.2	44.4	7.5	5.8	5.7	21.4	17.7	28.2
		Ccp		0.4	0.3	0.9	3.2	1.5	7.3	3.5	1.2	0.3	4.1	88.5	11.3
		Total BMS		90.7	88.1	46.1	94.5	4.6	86.9	37.1	9.5	71.2	32.2	111.9	71.3

Note: the weight percent of some elements has been normalized to 100% when the mass-balance calculations are more than 100%.

early at high temperature directly from the sulfide melt before MSS and ISS formations, such as within the Platreef at Turfspruit, Bushveld (Hutchinson and McDonald, 2008) and the Creighton deposit, Sudbury (Dare et al., 2010a). The Pt- and Pd-bearing discrete PGMs can also crystallize very late from the residual sulfide liquid during ISS crystallization when Te and Bi are enriched in the sulfide liquid (Holwell and McDonald, 2007). For the Jinchuan samples, the very fine Ir-bearing sulfur-arsenides are enclosed predominantly in the pentlandite indicating that they should be formed during the exsolution of pentlandite from MSS (Fig. 9). On the other hand, previous studies have shown that all PGE have stronger affinities for the As-bearing PGM than for sulfide phases (Godel et al., 2012; Hanley, 2007; Helmy et al., 2010; Wood, 2003). As a result, the Ir-bearing (+Rh) sulfur-arsenide should not crystallize before MSS crystallization (Fig. 9a–b), because Re, Os, Ru and Pd are mainly hosted in BMS (in pentlandite and pyrrhotite) rather than in As-bearing PGM in the net-textured

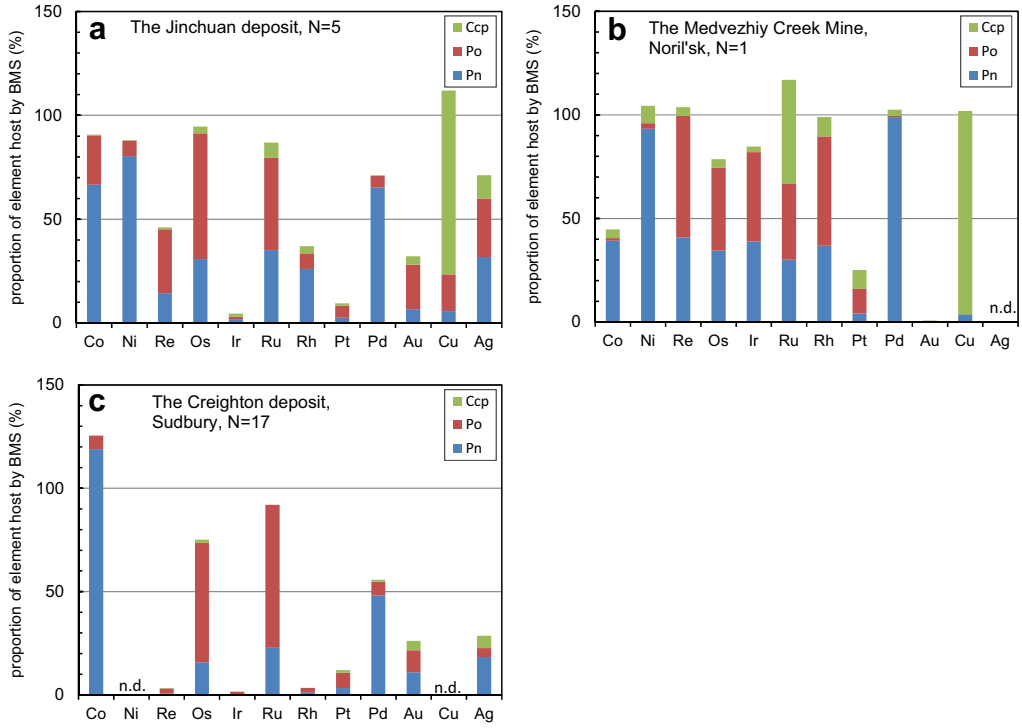

Fig. 7. Mass balance of the PGE and chalcophile elements in BMSfrom (a) the Jinchuan deposit (this study), (b) the Medvezhiy Creek Mine, Noril'sk (Barnes et al., 2006, 2008), and (c) the Creighton deposit, Sudbury (Dare et al., 2010a), plotted as the proportion (%) of each element in pyrrhotite (Po), pentlandite (Pn), and chalcopyrite (Ccp). N number of samples analyzed that have altered BMS, n.d. = not detected.

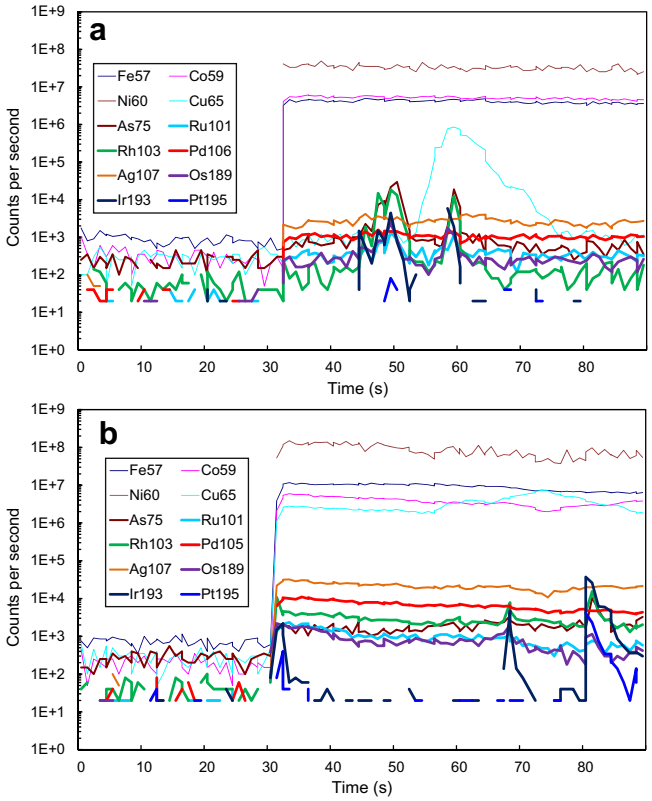

Fig. 8. Selected time-resolved laser spectra for PGE and other elements in (a) pentlandite with Ir–(Rh)–As–S microinclusion, and (b) pentlandite with Ir–Rh–(Pt)–As microinclusion from net-textured and massive ores obtained by LA-ICP-MS.

and massive ores, which are lower in PPGE than the Cu-rich ores. In contrast to IPGE, most Pt and a small portion of Pd exsolved from the Cu-rich residual sulfide liquid to form Pt- and Pd-bearing PGMs at low temperature (<650 °C, Fig. 9c, see next section in detail).

6.4. Decoupling between Pd and Pt

It is surprising that a large proportion of Pd (~65%) is partitioned into pentlandite instead of chalcopyrite, because Pd is an incompatible element in MSS and would be expected to concentrate in the residual sulfide liquid (Fig. 9b), form which chalcopyrite crystallizes (Cabri, 1973; Ebel and Naldrett, 1996, 1997; Kullerud et al., 1969; Misra and Fleet, 1973).

It is commonly agreed that pentlandite is originated from the exsolution of MSS (Cabri, 1973; Kelly and Vaughan, 1983; Kullerud et al., 1969; Misra and Fleet, 1973), although Peregoedova and Ohnenstetter (2002) proposed that pentlandite can exsolve from the fractionated Cu-rich liquid, via exsolution from heazlewoodite-ISS. The phenomena at Jinchuan are consistent with the former model. Firstly, the net-textured and massive ores are characterized by high IPGE contents and low Pd/Ru ratios, suggesting that these ores represent the mixture of MSS accumulation and interstitial sulfides (Chen et al., 2013). Secondly, our results reveal that Os, Ir, Ru and Rh are enriched in both pentlandite and pyrrhotite and approximately equally distributed between coexisting them (Fig. 7a). These are not consistent with late exsolution of pentlandite from the ISS, which is incompatible in these elements.

Consequently, we suggest that the high Pd concentration in pentlandite is a result of the diffusion of Pd into the pentlandite exsolved from MSS from the residual sulfide liquid on cooling (Fig. 9c). Barnes et al. (2006) had attributed the large amount of Pd in pentlandite from the Medvezhiy Creek Mine sulfide droplets in Noril'sk to Pd diffusion from ISS and MSS into pentlandite. The diffusion model is

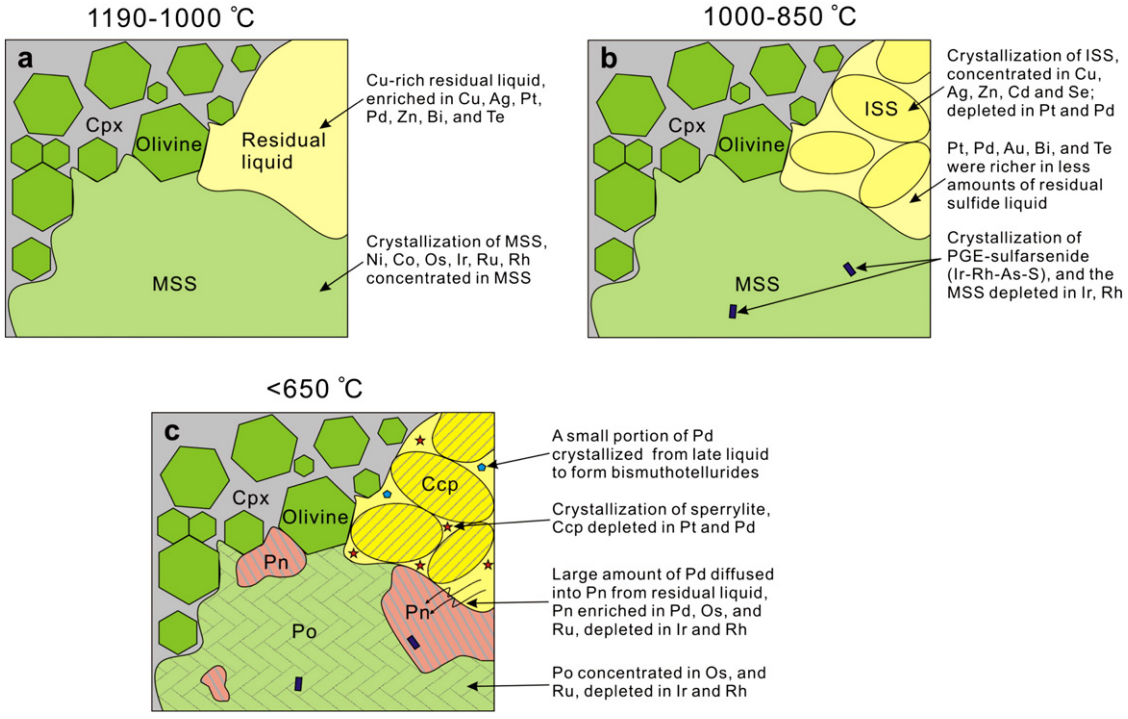

Fig. 9. Model of the processes that control the distribution of PGE and chalcophile elements among BMS and PGM in the Jinchuan deposit. (a) Crystallization of monosulfide solid solution (MSS), IPGE, Ni, and Co enriched in the MSS, and the remaining elements concentrated into the residual sulfide liquid; (b) crystallization of PGE sulfarsenides (Ir–Rh–As–S) directly from the MSS; crystallization of intermediate solid solution (ISS) from the Cu-rich melt and PPGE, Au, Bi and Te were richer in less amounts of residual liquid; (c) exsolution of pentlandite (Pn) and pyrrhotite (Po) from MSS and chalcopyrite (Ccp) from ISS. Large amount of Pd diffused into pentlandite from residual liquid, and crystallization of sperrylite ($PtAs_2$) and Pd-bismuthotelluride from residual liquid at low temperature.

consistent with experimental studies which have demonstrated that the solubility of Pd in MSS decreases from high temperature (up to 11 wt.% at 900 °C) to low temperature (~0.4 wt.% at 500 °C) (Makovicky et al., 1986), and therefore Pd enter pentlandite structure. At Jinchuan, the pentlandite grains grew at the margins of the pyrrhotite due to the exsolution of MSS during temperature decrease. The residual sulfide liquid will be further enriched in PPGE due to the crystallization of ISS in which PPGE is incompatible neither (Peregoedova, 1998). Therefore, Pd could diffuse into the growing pentlandite from the residual sulfide liquid to substitute Ni and result in the high Pd concentration in pentlandite (Fig. 9c). The strong correlation between Pd (and Co) and Ni is consistent with such a speculation that Pd is substituting for Ni in the pentlandite (Fig. 3). Additionally, the LA-ICP-MS results of PGE distribution in the BMS agree well with the above diffusion model. Firstly, the concentration of Pd in pentlandite from the net-textured and massive ores is higher than those from the disseminated ores, suggesting that high Pd in MSS cumulates may originate from the Cu-rich liquid trapped in the cumulate. Secondly, Pd contents in pentlandite from samples JC06-802 and GJ08-58-11, both of which contain a higher proportion of chalcopyrite, are higher than those in sample JC06-806 which has a lower proportion of chalcopyrite, implying that Cu-rich residual sulfide liquid provided an extra source of Pd. In addition, the late-forming flame of pentlandite (grains 2 and 7 in GJ08-58-11) is significantly poorer in Pd (and Co) relative to the granular pentlandite in the same sample (grains 1, 3 to 6 in GJ08-58-11, Table 2), further indicating that Pd could diffuse from Cu-rich sulfide liquid.

In contrast to Pd, Pt cannot be accommodated by any specific BMS and remains in the residual sulfide liquid together with other incompatible elements, such as As, Te, and Bi. Fleet et al. (1993) concluded that As, Te and Bi segregate as a late residual liquid which scavenges Pt preferentially over Pd. Strong positive correlations between Pt and As, and Te and Bi in the Jinchuan sulfide ores suggest that Pt may have been preferentially extracted from the Cu-rich residual sulfide liquid to crystallize of Pt-bearing PGMs (Figs. 5b, 9c). Such residual sulfide liquid containing Pt-bearing minerals may move to somewhere to form Cu-rich ores (Chen et al., 2013). Consequently, the crystallization of Pt-bearing minerals and diffusion of Pd into pentlandite during its exsolution from the MSS lead to decoupling between Pd and Pt in the net-textured and massive ores.

7. Conclusion

1. The LA-ICP-MS analysis has revealed that in the Jinchuan deposit pentlandite contains the highest contents of PGE, Co, and Re, followed by pyrrhotite, whereas chalcopyrite only hosts a small amount of Ag but negligible PGE. Mass balance calculations show that Co and Pd are mainly concentrated in pentlandite, and Re, Os, Ru, Rh, and Ag are hosted in significant proportions in pentlandite and pyrrhotite, whereas Ir and Pt are mainly present in PGM.
2. The distributions of the PGE and chalcophile elements among the BMS in Jinchuan are results of their partitioning behavior during the fractionation of sulfide liquid and exsolution of MSS. Cobalt, Re, Os, Ru, and Rh were partitioned into MSS that exsolved to pentlandite and pyrrhotite. Copper and a small proportion of Ag remained in the residual sulfide liquid that formed chalcopyrite.
3. The Ir-bearing sulfarsenide exsolved from MSS after its crystallization, whereas sperrylite crystallized from the Cu-rich residual sulfide liquid as discrete minerals at low temperature. These resulted in Ir and Pt depletions in the BMS.
4. The enrichment of Pd in pentlandite is attributed to the diffusion of Pd from the Cu-rich residual sulfide liquid. This diffusion and the crystallization of Pt-bearing minerals result in decoupling between Pd and Pt in the net-textured and massive ores at Jinchuan.

Supplementary data to this article can be found online at http://dx.doi.org/10.1016/j.oregeorev.2014.07.011.

Acknowledgments

This study was supported by research fund of State Key Laboratory of Ore Deposit Geochemistry (SKLOG-ZY125-06), the CAS/SAFEA International Partnership Program for Creative Research Teams — (Intraplate Mineralization Research Team; KZZD-EW-TZ-20), and NSFC projects of China (41003022, 40973038 and 41172090). We greatly appreciate Dr. B. Godel and Dr. J.-F. Gao for their constructive comments and Professor M.-F. Zhou for efficient editorial handling. We also thank the assistance of Mr. D.-H. Ba, F.-G. Qiao, Y.-C. Ren, J.-P. Jiang, and S.-L. Zheng during the fieldwork.

References

Ballhaus, C., Sylvester, P., 2000. Noble metal enrichment processes in the Merensky Reef, Bushveld Complex. J. Petrol. 41, 545–561.
Ballhaus, C., Tredoux, M., Spath, A., 2001. Phase relations in the Fe–Ni–Cu–PGE–S system at magmatic temperature and application to massive sulphide ores of the Sudbury Igneous Complex. J. Petrol. 42, 1911–1926.
Barnes, S.J., Lightfoot, P.C., 2005. Formation of magmatic nickel sulfide ore deposits and processes affecting their copper and platinum group element contents. Economic Geology 100th Anniversary Volumepp. 179–214.
Barnes, S.J., Makovicky, E., Karup-Moller, S., Makovicky, M., Rose-Hansen, J., 1997. Partition coefficients for Ni, Cu, Pd, Pt, Rh and Ir between monosulphide solid solution and sulphide liquid and the implications for the formation of compositionally zoned Ni–Cu sulphide bodies by fractional crystallization of sulphide liquid. Can. J. Earth Sci. 34, 366–374.
Barnes, S.J., Cox, R.A., Zientek, M.L., 2006. Platinum-group element, gold, silver and base metal distribution in compositionally zoned sulfide droplets from the Medvezky Creek Mine, Noril'sk, Russia. Contrib. Mineral. Petrol. 152, 187–200.
Barnes, S.J., Prichard, H., Cox, R., Fisher, P., Godel, B., 2008. The location of the chalcophile and siderophile elements in platinum-group element ore deposits (a textural, microbeam and whole rock geochemical study): implications for the formation of the deposits. Chem. Geol. 248, 295–317.
Cabri, L.J., 1973. New data on phase relations in the Cu-Fe-S system. Econ. Geol. 68, 443–454.
Cabri, L.J., Laflamme, J.H.G., 1984. Mineralogy and distribution of platinum-group elements in mill products from Sudbury. In: Park, W.C., Hausen, D.M., Hagni, R.D. (Eds.), Proceedings, 2nd International Congress on Applied Mineralogy in the Minerals Industry. American Institute of Mining and Metallurgy, vol. 2, pp. 911–922.
Cabri, L.J., Kojonen, K., Gervilla, F., Oberthür, T., Weiser, T., Johanson, B., Sie, S.H., Campbell, J. L., Teesdale, W.J., Laflamme, J.H.G., 2002. Comparison of PGE trace analyses of pentlandite and some arsenides and sulfarsenides by EPMA and Micro-PIXE. Ninth International Platinum Symposium, Program Abstracts, pp. 73–76.
Cabri, L.J., Sylvester, P.J., Tubrett, M.N., Peregoedova, A., Laflamme, J.H.G., 2003. Comparison of LAM-ICP-MS and Micro-PIXE results for palladium and rhodium in selected samples of Noril'sk and Talnakh sulfides. Can. Mineral. 41, 321–329.
Cabri, L.J., Choi, Y., Nelson, M., Tubrett, M., Sylvester, P.J., 2010. Advances in precious metal trace element analyses for deportment using LAM-ICP-MS. Proceedings of the 42nd Annual Canadian Mineral Processors Conference, pp. 181–196.
Chai, G., Naldrett, A.J., 1992a. Characteristics of Ni–Cu–PGE mineralization and genesis of the Jinchuan deposit, northwest China. Econ. Geol. 87, 1475–1495.
Chai, G., Naldrett, A.J., 1992b. The Jinchuan ultramafic intrusion, cumulate of a high-Mg basaltic magma. J. Petrol. 33, 277–303.
Chai, G., Naldrett, A.J., Rucklidge, J.C., Kilius, L.R., 1993. In situ quantitative analyses for PGE and Au in sulfide minerals of the Jinchuan Ni–Cu deposit by accelerator mass spectrometry. Can. Mineral. 31, 19–30.
Chen, L.M., Song, X.Y., Danyushevsky, L.V., Xiao, J.F., Li, S.B., Guan, J.X., 2009a. Correlation between Ni and MgO contents of olivine in Segment I of the Jinchuan intrusion, NW China, and its geological implication. Acta Petrol. Sin. 25, 3369–3378.
Chen, L.M., Song, X.Y., Danyushevsky, L.V., Xiao, J.F., Zhu, D., Zhou, G.F., Guan, J.X., Liu, S.R., Zheng, W.Q., 2009b. MELTS thermodynamic calculation of compositions of parental magma and fractional crystallization of the Jinchuan Intrusion, Gansu Province. Acta Geol. Sin. 83, 1302–1315.
Chen, L.M., Song, X.Y., Keays, R.R., Tian, Y.L., Wang, Y.S., Deng, Y.F., Xiao, J.F., 2013. Segregation and fractionation of magmatic Ni–Cu–PGE sulfides in the Western Jinchuan intrusion, NW, China: insights from platinum-group element geochemistry. Econ. Geol. 108, 1793–1811.
Danyushevsky, L., Robinson, P., McGoldrick, P., Large, R., Gilbert, S., 2003. LA-ICPMS of sulphides: evaluation of an XRF glass disc standard for analysis of different sulphide matrixes. 2003 Goldscmidt Conference, Japan. Geochim. Cosmochim. Acta, 67, A73 Suppl.
Danyushevsky, L., Robinson, P., Gilbert, S., Norman, M., Large, R., McGoldrick, P., Shelley, M., 2011. Routine quantitative multi-element analysis of sulphide minerals by laser ablation ICP-MS: standard development and consideration of matrix effects. Geochem. Explor. Environ. Anal. 11, 51–60.
Dare, S.A.S., Barnes, S.J., Prichard, H., 2010a. The distribution of platinum group elements (PGE) and other chalcophile elements among sulfides from the Creighton Ni–Cu–PGE sulfide deposit, Sudbury, Canada, and the origin of palladium in pentlandite. Miner. Deposita 45, 765–793.
Dare, S.A.S., Barnes, S.J., Prichard, H.M., Fisher, P.C., 2010b. the timing and formation of platinum-group minerals from the Creighton Ni–Cu–Platinum-group element sulfide

deposit, Sudbury, Canada: early crystallization of PGE-rich sulfarsenides. Econ. Geol. 105, 1071–1096.
Dare, S.A.S., Barnes, S.J., Prichard, H.M., Fisher, P.C., 2011. Chalcophile and platinum-group element (PGE) concentrations in the sulfide minerals from the McCreedy East deposit, Sudbury, Canada, and the origin of PGE in pyrite. Miner. Deposita 46, 381–407.
Dare, S.A.S., Barnes, S.J., Prichard, H.M., Fisher, P.C., 2014. Mineralogy and geochemistry of Cu-rich ores from the McCreedy east Ni–Cu–PGE deposit (Sudbury, Canada): implications for the behavior of platinum group and chalcophile elements at the end of crystallization of a sulfide liquid. Econ. Geol. 109, 343–366.
Ebel, D.S., Naldrett, A.J., 1996. Fractional crystallization of sulfide ore liquids at high temperature. Econ. Geol. Bull. Soc. 91, 607–621.
Ebel, D.S., Naldrett, A.J., 1997. Crystallization of sulfide liquids and the interpretation of ore composition. Can. J. Earth Sci. 34, 352–365.
Fleet, M.E., Chryssoulis, S.L., Stone, W.E., Weisener, C.G., 1993. Partitioning of platinum-group elements and Au in the Fe–Ni–Cu–S system: experiments on the fractional crystallization of sulfide melt. Contrib. Mineral. Petrol. 115, 36–44.
Fleet, M.E., Crocket, J.H., Stone, W.E., 1996. Partitioning of platinum-group elements (Os, Ir, Ru, Pt, Pd) and gold between sulfide liquid and basalt melt. Geochim. Cosmochim. Acta 60, 2397–2412.
Gilbert, S., Danyushevsky, L., Robinson, P., Wohlgemuth-Ueberwasser, C., Pearson, N., Savard, D., Norman, M., Hanley, J., 2013. A comparative study of five reference materials and the Lombard meteorite for the determination of the platinum-group elements and gold by LA-ICP-MS. Geostand. Geoanal. Res. 37, 51–64.
Godel, B., Barnes, S.J., 2008. Platinum-group elements in sulfide minerals and the whole rocks of the J–M Reef (Stillwater Complex): implication for the formation of the reef. Chem. Geol. 248, 272–294.
Godel, B., Barnes, S.J., Maier, W.D., 2007. Platinum-group elements in sulphide minerals, platinum-group minerals, and whole-rocks of the Merensky Reef (Bushveld Complex, South Africa): implications for the formation of the reef. J. Petrol. 48, 1569–1604.
Godel, B., González-Álvarez, I., Barnes, S.-J., Barnes, S.J., Parker, P., Day, J., 2012. Sulfides and sulfarsenides from the Rosie Nickel Prospect, Duketon Greenstone Belt, Western Australia. Econ. Geol. 107, 275–294.
Guillong, M., Danyushevsky, L., Waelle, M., Raveggi, M., 2011. The effect of quadrupole ICPMS interface and ion lens design on argide formation: implications for LA-ICPMS analysis of PGE's in geological samples. J. Anal. At. Spectrom. 26, 1401–1407.
Hanley, J.J., 2007. The role of arsenic-rich melts and mineral phases in the development of high-grade Pt–Pd mineralization within komatiite-associated magmatic Ni–Cu sulfide horizons at Dundonald Beach South, Abitibi subprovince, Ontario, Canada. Econ. Geol. 102, 305–317.
Helmy, H.M., Ballhaus, C., Wohlgemuth-Ueberwasser, C., Fonseca, R.O.C., Laurenz, V., 2010. Partitioning of Se, As, Sb, Te and Bi between monosulfide solid solution and sulfide melt — application to magmatic sulfide deposits. Geochim. Cosmochim. Acta 74, 6174–6179.
Holwell, D.A., McDonald, I., 2007. Distribution of platinum-group elements in the Platreef at Overysel, northern Bushveld Complex, a combined PGM and LA-ICP-MS study. Contrib. Mineral. Petrol. 154, 171–190.
Hutchinson, D., McDonald, I., 2008. Laser ablation ICP-MS study of platinum-group elements in sulphides from the Platreef at Turfspruit, northern limb of the Bushveld Complex, South Africa. Miner. Deposita 43, 695–711.
Jinchuan Nonferrous Metal Corporation, 1997. Study on the geological features and mineralization of the unexposed Cu-rich ore body in Segment I at Jinchuan, unpublished.
Jinchuan Nonferrous Metal Corporation, 2003. The final report of the engineering geology at 1160 level on I-8 exploration line of Segment I, unpublished.
Kelly, D., Vaughan, D., 1983. Pyrrhotine–pentlandite ore textures, a mechanistic approach. Mineral. Mag. 47, 453–463.
Kullerud, G., Yund, R.A., Moh, G.H., 1969. Phase relations in the Cu–Fe–S, Cu–Ni–S, and Fe–Ni–S systems. Econ. Geol. Monogr. 4, 323–343.
Lehmann, J., Arndt, N., Windley, B., Zhou, M.F., Wang, C.Y., Harris, C., 2007. Field relationships and geochemical constraints on the emplacement of the Jinchuan intrusion and its Ni–Cu–PGE sulfide deposit, Gansu, China. Econ. Geol. 102, 75–94.
Li, C., Barnes, S.J., Makovicky, E., Rose-Hansen, J., Makovicky, M., 1996. Partitioning of nickel, copper, iridium, rhenium, platinum, and palladium between monosulfide solid solution and sulfide liquid: effects of composition and temperature. Geochim. Cosmochim. Acta 60, 1231–1238.
Li, X.H., Su, L., Chung, S.L., Li, Z.X., Liu, Y., Song, B., Liu, D.Y., 2005. Formation of the Jinchuan ultramafic intrusion and the world's third largest Ni–Cu sulfide deposit: associated with approximately 825 Ma south China mantle plume? Geochem. Geophys. Geosyst. 6, Q1104. http://dx.doi.org/10.1029/2005GC001006.
Longerich, H.P., Jackson, S.E., Günther, D., 1996. Laser ablation inductively coupled plasma mass spectrometric transient signal data acquisition and analyte concentration calculation. J. Anal. At. Spectrom. 11, 899–904.
Makovicky, M., Makovicky, E., Rose-Hansen, J., 1986. Experimental studies on the solubility and distribution of platinum-group elements in base metal sulphides in platinum deposits. In: Gallagher, M.J., Ixer, R.A., Neary, C.R., Pritchard, H.M. (Eds.), Metallurgy of Basic and Ultrabasic Rocks. Institute of Mining and Metallurgy, London, pp. 415–425.
McDonough, W.F., Sun, S.S., 1995. The composition of the earth. Chem. Geol. 120, 223–253.
Misra, K., Fleet, M.E., 1973. The Chemical Compositions of Synthetic and Natural Pentlandite Assemblages. Econ. Geol. 68, 518–539.
Mungall, J.E., Andrews, D.R.A., Cabri, L.J., Sylvester, P.J., Tubrett, M., 2005. Partitioning of Cu, Ni, Au, and platinum-group elements between monosulfide solid solution and sulfide melt under controlled oxygen and sulfur fugacities. Geochim. Cosmochim. Acta 69, 4349–4360.
Naldrett, A.J., 2004. Magmatic Sulfide Deposits, Geology, Geochemistry and Exploration. Springer (727 pp.).
Peregoedova, A.V., 1998. The experimental study of the Pt–Pd-partitioning behavior between monosulfide solid solution and Cu–Ni-sulfide melt at 900–840 °C. 8th International Platinum Symposium Abstracts. Geol. Soc. South Africa and South African Institute of Mining and Metallurgy Symposium Series, S18, pp. 325–327.
Peregoedova, A., Ohnenstetter, M., 2002. Collectors of Pt, Pd and Rh in a S-poor Fe–Ni–Cu sulfide system at 760 °C, experimental data and application to ore deposits. Can. Mineral. 40, 527–561.
Piña, R., Gervilla, F., Barnes, S.J., Ortega, L., Lunar, R., 2012. Distribution of platinum-group and chalcophile elements in the Aguablanca Ni–Cu sulfide deposit (SW Spain): evidence from a LA-ICP-MS study. Chem. Geol. 302–303, 61–75.
Prichard, H., Knight, R., Fisher, P., McDonald, I., Zhou, M.-F., Wang, C., 2013. Distribution of platinum-group elements in magmatic and altered ores in the Jinchuan intrusion, China: an example of selenium remobilization by postmagmatic fluids. Miner. Deposita 48, 767–786.
Qi, L., Zhou, M.-F., Wang, C.Y., Sun, M., 2007. Evaluation of a technique for determining Re and PGEs in geological samples by ICP-MS coupled with a modified Carius tube digestion. Geochem. J. 41, 407–414.
Sixth Geological Unit, 1984. Geology of the Baijiaozuizi Cu–Ni sulfide deposit. Geological Survey of Gansu ProvinceGeological publishing House, Beijing.
Song, X.-Y., Zhou, M.-F., Wang, C.-Y., Qi, L., Zhang, C.-J., 2006. Role of crustal contamination in formation of the Jinchuan intrusion and its world-class Ni–Cu–(PGE) sulfide deposit, northwest China. Int. Geol. Rev. 48, 1113–1132.
Song, X.-Y., Keays, R.R., Zhou, M.-F., Qi, L., Ihlenfeld, C., Xiao, J.-F., 2009. Siderophile and chalcophile elemental constraints on the origin of the Jinchuan Ni–Cu–(PGE) sulfide deposit, NW China. Geochim. Cosmochim. Acta 73, 404–424.
Song, X.-Y., Danyushevsky, L., Keays, R., Chen, L.-M., Wang, Y.-S., Tian, Y.-L., Xiao, J.-F., 2012. Structural, lithological, and geochemical constraints on the dynamic magma plumbing system of the Jinchuan Ni–Cu sulfide deposit, NW China. Miner. Deposita 47, 277–297.
Su, S., Li, C., Zhou, M.-F., Ripley, E., Qi, L., 2008. Controls on variations of platinum-group element concentrations in the sulfide ores of the Jinchuan Ni–Cu deposit, Western China. Miner. Deposita 43, 609–622.
Tang, Z.L., Li, W.Y., 1995. Mineralization Model and Geology of the Jinchuan PGE-bearing Deposit. Geological Publishing House, Beijing.
Wood, M. 2003. Arsenic in igneous systems: An experimental investigation, unpublished B.A. Sc. Thesis, Toronto Univ., 34 p.
Yang, X.Z., Ishihara, S., Zhao, D.H., 2006. Genesis of the Jinchuan PGE deposit, China: evidence from fluid inclusions, mineralogy and geochemistry of precious elements. Miner. Petrol. 86, 109–128.
Zhang, M., Kamo, S., Li, C., Hu, P., Ripley, E., 2010. Precise U–Pb zircon–baddeleyite age of the Jinchuan sulfide ore-bearing ultramafic intrusion, Western China. Miner. Deposita 45, 3–9.